Journal of Optoelectronics and Advanced Materials Vol. 4, No. 3, September 2002, p. 649 - 664

INVESTIGATION OF CHALCOGENIDE GLASSY SEMICONDUCTORS IN THE BEN-GURION UNIVERSITY (ISRAEL)

V. M. Lyubin[*], M. L. Klebanov

Department of Physics, Ben-Gurion University of the Negev, Beer-Sheva 84105, Israel

The study of chalcogenide glassy semiconductors (ChGS) in the Ben-Gurion University (Israel) started in early 1992 and was based on the results obtained in the A. F. Ioffe Physico-Technical Institute (St. Petersburg, Russia). Most investigations were performed in the following directions: structural transformations induced by short intense light pulses, photoinduced optical anisotropy, photoinduced electrical anisotropy, polarization-dependent anisotropic photocrystallization, Zn-photodoping, application of ChGS for development of microlens arrays and photonic band-gap structures. Main results of these investigations are reviewed shortly in this paper.

(Received May 27, 2002; accepted July 22, 2002)

Keywords: Chalcogenide, Anisotropy, Zn-doping, Microlens array, Photonic band-gap structure

1. Structural transformations induced by short intense light pulses

Photoinduced structural transformations in chalcogenide glassy semiconductors have been studied extensively during the last two decades [1-4]. In spite of the great number of accomplishments (see recent review papers [5, 6]), many details of this phenomenon continue to be vague. One of the most interesting peculiarities of photostructural transformations is a huge increase of photosensitivity in the case of short intense pulsed light excitation [7-10], reaching a factor of hundreds. This effect is very important for practical applications as it overcomes the main drawback of this class of very high resolution photorecording and photoresist materials, namely their relatively small photosensitivity. Up to now there is no general agreement on the mechanism of this photosensitivity increase. Different researchers speak about the thermal [8], photothermal [9] or non-thermal [7,10,11] nature of this effect.

In most cases, the after-effect of pulse excitation (the “after-pulse” effect) was studied by considering the change of chalcogenide sample properties (absorption coefficient, refractive index or rate of dissolution in some selective solvents) several minutes or several tens of minutes after the pulse excitation. Only Aoyagi et al [11] and Keiji Tanaka [12] examined the dynamic behavior of photostructural transformations in As_2S_3 glassy films.

In our researches [13-16] we investigated both the after-pulse effect and the dynamic characteristics of photostructural transformations induced in several ChGS films by intense nanosecond laser pulses. The data indicate that the strong increase of photosensitivity following short intense light pulses is due to a multi-photon effect that eases the process of structural rearrangement.

Glassy As-Se, As-S and As-Se-Te films of 0.3-1.0 μm thickness were prepared by evaporation of crushed bulk chalcogenide glass in a vacuum of $(2\text{-}5) \times 10^{-6}$ Torr from a quartz crucible onto oxide glass substrates.

---

[*] Prof. Victor M. Lyubin is the winner of the Stanford R. Ovshinsky Award for Excellence in Non-Crystalline Chalcogenides for 2002.

In our experiments we used short intense pulses of different lasers and compared the action of these pulses with the action of CW radiation. Comparison of single ArF laser pulse (16 ns, 0.5-4.5 mJ) with CW He-Ne laser radiation is demonstrated in Fig. 1. It is seen that the sensitivity of photodarkening in the former case is about 1500 times larger. Approximately the same results were obtained when short intense pulses (5 ns, 3-5 mJ) of Nd;YAG laser were used for the films excitation. A single KrF laser pulse (16 ns, 15 mJ) induced marked photodarkening in As-Se-Te films. In this case we observed more than 6000 times higher sensitivity. All properties of photodarkened film areas did not depend on the mode of excitation, pulse or CW. For example, in both cases the "erasing" of written spots could be fulfilled by heating the film to the same temperature, and the irradiated areas were dissolved in proper solvents with the same rate. All these data prove the similar nature of the photodarkened state of the films after pulse and CW irradiation.

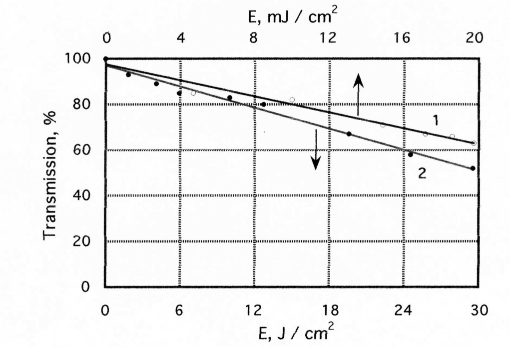

Fig. 1. Change of transmission of ~ 0.4 μm As-Se film as a function of radiation of pulsed ArF laser (1) and CW He-Ne laser (2).

The after-pulse effect was also studied using for excitation the short pulses (5 ns, up to 50 mJ/cm^2 fluence) of a frequency doubled Nd:YAG laser (λ = 532 nm). The dynamic characteristics of photostructural transformations were investigated by the transient-grating method [11]. The laser writing beam (70 mJ/cm^2 maximum fluence) was separated into two equal intensity beams that interfere on the sample, writing a grating of period ~ 1.5 μm. A weak CW He-Ne laser beam was sent normal to the sample in order to probe the grating formation. A high-speed photomultiplier (~1 ns response time) detected probe light diffracted by the grating. The detector was linked to a digital oscilloscope and data were transferred to a PC for processing.

A dual time scale behavior was observed. As it is shown in Fig. 2a, a sharp and short peak with a time scale of a few tens of nanoseconds (the “transient pulse”) was followed by a slow (a few microseconds) increase of the signal that asymptotically reached a constant value (the after-pulse value). If the transient and the after-pulse signals (shown in Fig. 2a) are plotted as a function of the writing beam fluence, one obtains a very different behavior, as illustrated on a log-log scale in Fig. 2b: the transient signal has a slope of ~1.75 ± 0.5 whereas the after-pulse signal has a slope of 4.5 ± 1.0. Since the grating efficiency scales as the square of the writing beam fluence, this suggests a transient effect that behaves linearly and an after-pulse effect, that behaves quadratically with the writing beam fluence. In order to overcome pulse-to- pulse and sample-to-sample variations, we have directly plotted the after-pulse signal as a function of the transient signal in a log-log scale (Fig. 3), and obtained by linear fit a slope of 2.29.

The transient behavior is compatible with results obtained by other groups [12]. However, the quadratic dependence of the after-pulse photodarkening kinetics in the case of pulsed excitation suggests a two-photon or two-electron process analogous to a bimolecular reaction. To the best of our knowledge, this is the first observation of this kind of nonlinear behavior in chalcogenide glasses.

First let us explain the existence of the dual time scale behavior and the proportionality of the short transient with the writing beam fluence. Free electrons (holes) excited by the interfering light beams locally change the refractive index and the absorption of the chalcogenide glass and create an initial diffractive grating. This grating is both a phase and absorption grating. However both causes are due to the creation of free electrons, and the He-Ne light probes this electronic process. Then, the charge carriers start to diffuse within the material due to the density gradient. It takes them a few tens of nanoseconds to be thermalized within the material. During this time, the initial transient grating disappears, and one observes a transient decay that in fact provides direct information on the diffusion constant of carriers in the chalcogenide glass studied [11,12]. The electron density is directly proportional to the writing beam fluence, and thus, one observes a quadratic relationship between the diffracted beam and the writing beam fluence.

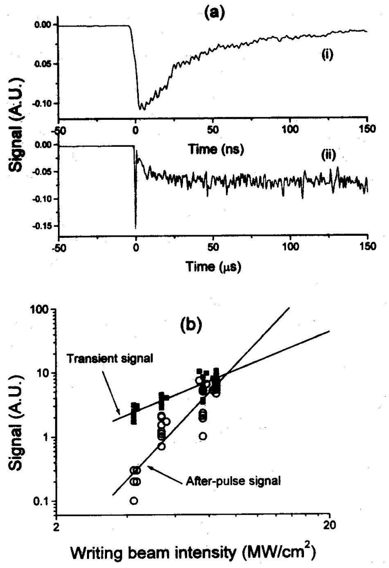

Fig. 2. (a) Typical diffracted signal. A few tens of nanoseconds transient (i) is followed by a slow asymptotic response, the after - pulse effect (ii). The transient starts with the exciting pulse. (b) Diffracted signal as a function of the writing beam intensity.

More interesting are the after-pulse processes that lead to the recorded hologram stable in time (holographic memory). These processes are due to the photoinduced structural transformations characteristic of ChGS [1-6]. Part of the excited free charge carriers are captured by special trapping centers modifying a local atomic arrangement (trapping excitons [16]) and leading to large change of optical, photoelectric and chemical properties of the chalcogenide film. This process of structural transformations proceeds much slower than the first one that involves only electronic excitation, transport and recombination.

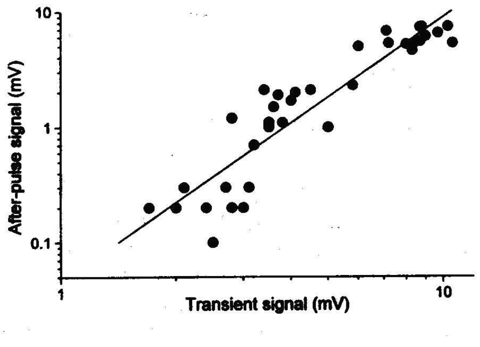

Fig. 3. After-pulse signal as a function of the transient signal, for the same excitation pulse.

We propose the following model to explain this after-pulse behavior. Let us call **A** atomic sites where one electron has been trapped. The local atomic conformation can relax to two states: either to state **I,** the initial atomic conformation, or to state **F** (double well model [12]). The probability of transition to state **F** is much lower than to state **I**. However, if two sites **A** are close enough they form a complex **B** which can rearrange with a much higher probability to the state **F**. We can call the latter processes a two-photon process. Usually this term is used when the energy of a single photon is not enough to excite an electron to the conductivity band, and only two photons are capable to accomplish such process. In our case, each single photon has enough energy to produce a free electron-hole pair but such excitation does not lead to creation of the state **F**.

Generation of state **A** is accompanied by the weakening or even breaking of the interatomic bonds in the chalcogenide film but subsequent relaxation restores with large probability the initial bonding configuration **I**. Only when two photons weaken or break the neighboring bonds, does the probability of the creation of state **F** (stable structural transformation) increase significantly.

At low writing beam fluence, **A** sites are too far from each other to give **B**, and the writing efficiency is small. Such a situation is usually found in the case of CW excitation. In case of high writing beam fluence, **A** sites are sufficiently close to each other in order to form **B**, and the writing efficiency is much higher.

In conclusion, this investigation of the dynamic characteristics of photostructural transformations induced in glassy $As_{50.}Se_{50}$ films by nanosecond Nd:YAG laser pulses suggests that the strong increase of photosensitivity in case of short intense light pulses excitation in comparison with CW excitation is due to a two-photon effect. If two photons are absorbed close to each other and weaken or break the neighboring interatomic bonds of the chalcogenide glass, the process of structural rearrangement proceeds with much larger probability and this process can be realized only at large enough writing beam fluences. These results show that ChGS films are very prospective materials for pulsed holography, pulsed photorecording and pulsed photolithography.

2. Photoinduced optical anisotropy

The phenomenon of photoinduced anisotropy (PA) was discovered when we studied the polarization state of light transmitted through the film of chalcogenide glassy semiconductor (ChGS), irradiated by the linearly polarized laser beam [17, 18]. Both photoinduced dichroism and photoinduced birefringence of absorption, observed in that experiments, were explained by interaction of light with optically anisotropic structural elements whose optical axes are oriented randomly. Later, these phenomena were investigated by different authors, worked with ChGS films and bulk samples of various compositions [19-26]. Different approaches to explain the mechanism of PA were developed [23-28].

Here we consider the results of the PA study accomplished recently in the amorphous semiconductors laboratory of the Ben-Gurion University (Beer-Sheva, Israel) either independently or in close cooperation with colleagues from other research centers. It is convenient to divide all obtained data into the parts concerning the photoinduced anisotropic absorption, reflection and scattering of light.

Two groups of samples were investigated in this research. Thin-film samples were produced by thermal evaporation of starting glassy materials onto silica glass substrates in vacuum ($p\sim10^{-6}$ Torr). The film thickness was 0.3-4.0 μm. Bulk samples were prepared by polishing of the melt-quenched chalcogenide glasses and had typical thickness of several millimeters. All measurements were done at room temperature using the experimental installations described in [29].

2.1. Anisotropic light absorption

In our recent research [30] we obtained the data which permit further development of Tikhomirov and Elliott`s model [23]. Studying the AsSe films, we demonstrated that the whole process of dichroism generation in the case of the above-band-gap light excitation can be divided into two subprocesses. The first process is the generation of some centers that can be oriented by the polarized light and the second one is the photostimulated orientation (and reorientation) of these centers.

The process of photoinduced dichroism appearance and reorientation in the AsSe film of 1.2 μm thickness at 2.75 W/cm^2 light intensity is illustrated in Fig. 4. It is seen that the initial dichroism generation is rather prolonged (10-20 min), while the dichroism reorientation happens much quicker (< 1 min.). Quick reorientation was observed not only after dichroism saturation, as it is shown in Fig.

4a, but also in the initial moments of dichroism growth. Moreover, in the case of long film irradiation with the unpolarized light, the following irradiation with linearly polarized light results in rapid appearance of dichroism as it is shown in Fig. 4b. Similar generation and reorientation processes were observed also in amorphous $As_{45}Se_{55}$, As_2S_3 and Ge_2PbS_4 films. We want to stress that a division into slow dichroism appearance and quick dichroism reorientation is especially distinct in the films of certain thickness and at certain values of exciting light intensity.

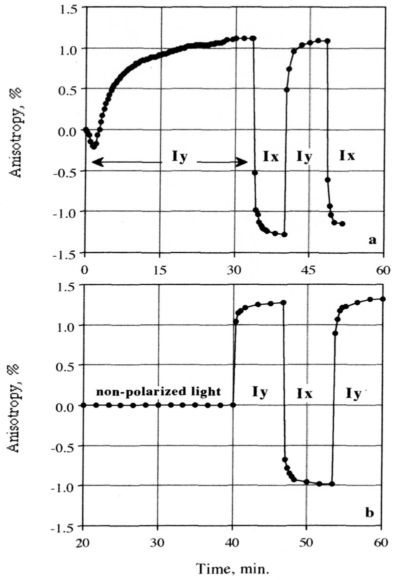

Fig. 4. Kinetics of dichroism generation and reorientation in AsSe film under the action of linearly polarized laser light with two orthogonal directions of electrical vector (y and x), when reorientation starts after dichroism saturation (a) or when polarized light irradiation starts after prolong illumination with non-polarized light (b).

Fig. 5 shows the room-temperature kinetics of repeated photoinduced dichroism generation after heating the film to a certain temperature, keeping it at this temperature and then cooling to room temperature. The kinetics of room-temperature dichroism reorientation in the non-annealed film is also shown. It is seen that the gradual increase of annealing temperature brings the form of the dichroism growing curve nearer to that in the virgin film, and practically perfect identity of the curves has place after annealing at temperature 180°C that is the softening temperature of the AsSe film. We want to remind that the total bleaching of photodarkened AsSe film was also observed at temperature close to the softening temperature, while the partial bleaching starts at lower temperatures [31].

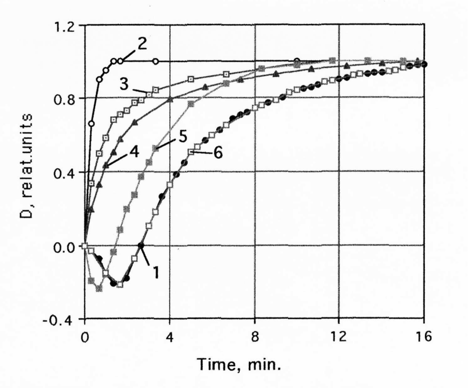

Fig. 5. Kinetics of room temperature dichroism (D) generation in virgin AsSe film of 1.2 μm thickness (1), repeated dichroism generation after annealing at 75 (3), 95 (4), 140 (5), 180 °C (6) and kinetics of one cycle of room temperature dichroism reorientation (2).

All above-described results show that irradiation with both polarized and non-polarized above-band-gap light creates some centers in the non-irradiated film that can be oriented quickly by the subsequent irradiation by linearly polarized light (in case of initial irradiation with the polarized light, these centers are oriented during this irradiation). The results of the heating experiments allow to think that the same centers (or, may be, some part of these centers that are capable to be oriented) are responsible for both the photodarkening and saturated value of PA. These centers can be born in the form of VAP`s in the reactions:

$$2C_2^0 + h\nu \rightarrow C_1^- + C_3^+ \text{ and } C_2^0 + P_3^0 + h\nu \rightarrow C_1^- + P_4^+, \qquad (1)$$

where C and P mean the chalcogen and pnictide atoms.

Combining the ideas proposed in [23] and [28], we assume that the polarized light initiates the reactions:

$$C_1^- + C_3^+ + h\nu \rightarrow C_1^+ + C_3^- \text{ and } C_1^- + P_4^+ + h\nu \rightarrow C_1^+ + P_4^-, \qquad (2)$$

and these reactions occur much more often in the VAP`s with dipole moment oriented in parallel to electrical vector of exciting light. Afterwards, the energetically advantageous reactions:

$$C_1^+ + C_3^- \rightarrow C_1^- + C_3^+ \text{ and } C_1^+ + P_4^- \rightarrow C_1^- + P_4^+ \qquad (3)$$

take place, but now the $C_1^- + C_3^+$ and $C_1^- + P_4^+$ defects are oriented randomly. The whole process is accompanied by the decrease of the number of VAP`s having the dipole moments co-directed with the electrical vector of the inducing light and by the growth of anisotropy that we have observed.

2.2. Anisotropic light scattering

The photoinduced light scattering in bulk ChGS, excited by the sub-band-gap light was revealed for the first time in [24]. This effect was displayed as a change of the shape of the transmitted laser beam, as an appearance of speckled structure and as a photoinduced modification of trace of the laser beam inside the irradiated ChGS bulk sample. Semi-quantitative data confirming the light scattering were also obtained [24]. In this research we investigated carefully the photoinduced light scattering in bulk glass and first of all, the anisotropy of light scattering. The obtained results allowed to propose some new ideas about the mechanism of the whole group of vectorial photoinduced phenomena in bulk ChGS [32].

He-Ne laser light ($h\nu = 1.96$ eV, W = 10 mW) which is a sub-band-gap radiation for an As_2S_3 glass ($E_g = 2.3$ eV) has been used in these experiments carried out at a room temperature. Study of the angular distribution of intensity of probing light transmitted through the sample (using a special movable diaphragm) before and after its irradiation with an exciting light beam, permitted to consider the light at the angles up to 5 mrad as a directly transmitted light and the light at larger angles as a scattered light.

We studied the kinetics of change of scattered light intensity induced by strong linearly polarized radiation with two orthogonal directions of electrical vector (E_y-radiation and E_x-radiation). It was shown that the E_y-radiation, for example, induces an increase of scattering of the corresponding (I_y light. Simultaneously, the intensity of I_x light usually decreases. On the contrary, the E_x-radiation induces a decrease of I_y light and a growth of I_x light.

Fig. 6 shows a typical kinetics of photoinduced changes of the scattered light anisotropy $2(I_{Sy} - I_{Sx}) / (I_{Sy} + I_{Sx})$ and of the transmitted light anisotropy $2(I_{ty} - I_{tx}) / (I_{ty} + I_{tx})$. It is seen from the figure that scattering anisotropy and transmittance anisotropy always change in opposite directions: an increase of one of them is accompanied by the decrease of the other one and vice versa. The anisotropy of scattering and transmittance were shown to remain practically invariant during at least 3 - 5 hours. It is concluded from the data of Fig. 6, that it is possible to reorient the PA.

In some experiments the sample was first excited by non-polarized light (E_y+E_x) and only then was irradiated by linearly polarized radiation. Non-polarized radiation induced additional isotropic light scattering, while the subsequent linearly polarized radiation led to the appearance of scattering anisotropy, and this anisotropy could be reoriented.

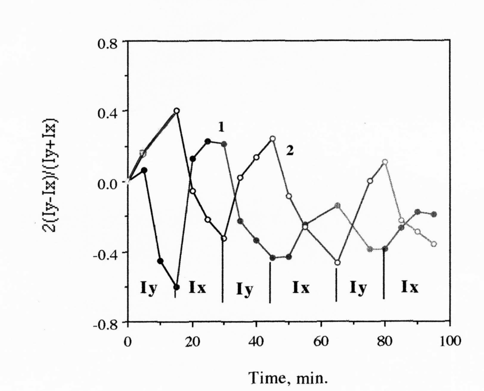

Fig. 6. Kinetics of transmission anisotropy (1) and scattering anisotropy (2) changes in an As_2S_3 bulk glass sample induced by E_y- and E_x-laser radiation.

Obtained quantitative data about the photo-induced light scattering anisotropy permit us to draw some interesting conclusions. The opposite directed changes of photoinduced anisotropy of transmittance and scattering allow us to assume that the creation of anisotropically scattering centers is the basis of the whole group of photoinduced vectorial phenomena in ChGS. This hypothesis makes understandable the fact that anisotropy is excited by the sub-band-gap light. The energy of corresponding light quanta is not sufficient to break the interatomic covalent bond, but enough to produce some changes in the system of weaker bonds, for example, intermolecular Van der Waals bonds. These changes can result in the appearance of scattering centers in the glass. Such centers will scatter the light either isotropically or anisotropically, depending on the polarization state of the inducing radiation. The anisotropy of such centers can be reoriented when the polarization state of the inducing radiation is changed. The different states of scattering centers (x-oriented, y-oriented, isotropic) reflect the possibility of certain structural fragments in the glass to exist in several quasi-stable states as was considered in the case of photodarkening in ChGS [31].

2.3. Anisotropic light reflection

All previous studies of PA in ChGS used the transmission measurements and for this reason only the effect of sub-band-gap and above-band-gap light was investigated. Interaction of ChGS with the photons having the energy substantially exceeding the optical gap of ChGS could not be studied because of strong absorption. Below we report the results of the reflectance-difference spectroscopy application which allowed us to investigate the photoinduced anisotropy in ChGS in a broad spectral range [33].

In all thin films and bulk glassy samples studied we recorded PA in the whole investigated spectral range (1.5-5.0 eV), while the non-irradiated samples were either completely optically isotropic or showed very slight anisotropy due to preparation conditions. On changing the exciting light polarization to orthogonal, the reflectance curve indicated a change in the anisotropy sign. Fig. 7 shows the PA of light reflection in the bulk As_2S_3 induced by the linearly polarized light of Xe lamp. It is seen that the anisotropy appeared in the whole 1.5-5.0 eV range. All peculiarities of PA of reflection were shown to be characteristic not only for As_2S_3 glass but also for all ChGS studied.

The possibility to observe PA at energies much larger than the exciting photon energy indicates that by irradiation of ChGS with linearly polarized light not only defects or the scattering centers can be oriented and reoriented by light but also the main covalent network of the glass becomes anisotropic, it means that the main interatomic covalent bonds can be also oriented and reoriented. The data on the anisotropy of reflection induced by the sub-band-gap and above-band-gap light can be understood in close analogy with the explanation given above.

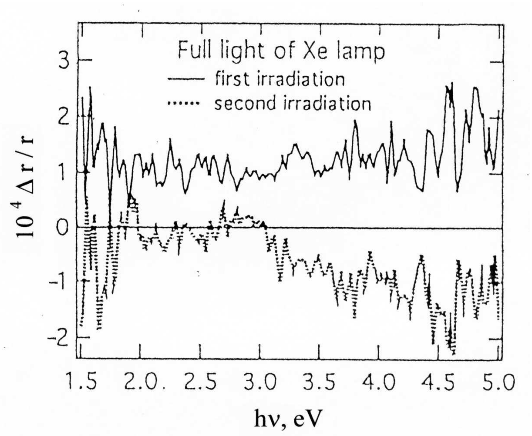

Fig. 7. Photoinduced reflectance anisotropy (solid line) and its reorientation (dotted line) in an As_2S_3 bulk glass sample irradiated by the light of 1000 W Xe-lamp.

The detailed investigation of interaction of linearly polarized light with ChGS allows us to conclude that a tendency to photoinduced macroanisotropy is a common property of these materials. It manifests in anisotropic light absorption, reflection and scattering which can be observed in different spectral ranges using various experimental techniques. The common base for this photoinduced macroanisotropy is the existence in ChGS of large number of micro-anisotropic fragments. In the non-irradiated ChGS such fragments are oriented randomly, making the samples optically macroisotropic. Polarized light leads to the redistribution of these fragments. Such general idea was suggested in the very first papers concerning the photoinduced anisotropy in ChGS [17,18]. One of possible cases of such redistribution was considered in detail by Fritzsche [28]. Moreover, our experiments demonstrated that not only natural fragments but also photoinduced fragments (defects) are microanisotropic and can be oriented and reoriented by the linearly polarized light. We are convinced now that different defects and even interatomic bonds can play the role of such microanisotropic fragments in ChGS that determine the anisotropy excited by the light of different spectral ranges: sub-band-gap, above-band-gap and super-band-gap light.

3. Photoinduced electrical anisotropy

Continuing our research, we succeeded to demonstrate that the photoinduced optical anisotropy excited in several amorphous chalcogenide films by linearly polarized laser beam is accompanied by the photoinduced anisotropy of photoconductivity [34, 35]. We investigated amorphous $As_{50}Se_{50}$, Sb_2S_3 and $Ge_{28.5}Pb_{15}S_{56..5}$ films having thickness in the range 0.3 - 2.0 μm. A set-up for study of photoconductivity is described in [34,35]. .

When the $As_{50}Se_{50}$ sample with two parallel electrodes was irradiated by a non-polarized He-Ne laser beam (a laser spot was set between electrodes), we detected appearance and subsequent saturation of photocurrent. Following irradiation by linearly polarized light with an electric vector E either parallel (Ex), or orthogonal (Ey) to electrodes resulted in appearance of anisotropy of photocurrent (Fig. 8). Values of anisotropy achieved ~ 0.5-1.0 %. This result was confirmed in experiments with three-electrodes samples allowed us to detect anisotropy of photoconductivity in more details. A change in the polarization state of the inducing light resulted in the respective change of the sign of dichroism. Kinetics of the change of resultant photo- current was similar to the kinetics of reorientation of the optical dichroism.

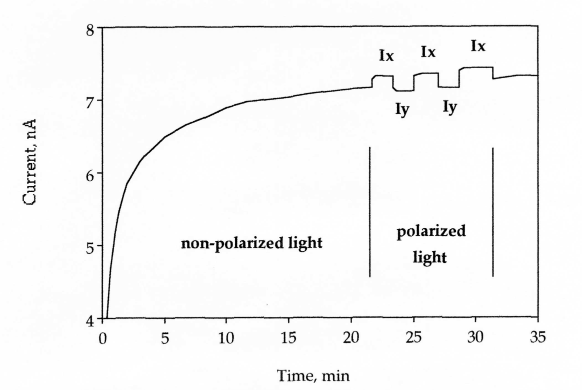

Fig. 8. Kinetics of photocurrent following the change of the polarization state E of the inducing beam of He-Ne laser in a two-electrodes AsSe sample.

Qualitatively similar results were obtained with amorphous Sb_2S_3 and $Ge_{28.5}Pb_{15}S_{56..5}$ films when using both the intense linearly polarized He-Ne and Ar+ laser beams. Kinetics of relative anisotropy ΔJ/J of photocurrent J in the 1.5 μm thick Sb_2S_3 film is shown in Fig. 9. It is seen that while variation of the inducing light polarization results in change of the sign of anisotropy, irradiation with circularly polarized light is accompanied by the gradual decrease of anisotropy to zero. It was shown that values of anisotropy of photocurrent in the Sb_2S_3 and $Ge_{28.5}Pb_{15}S_{56..5}$ films were 2-3 times larger than in the $As_{50}Se_{50}$ films.

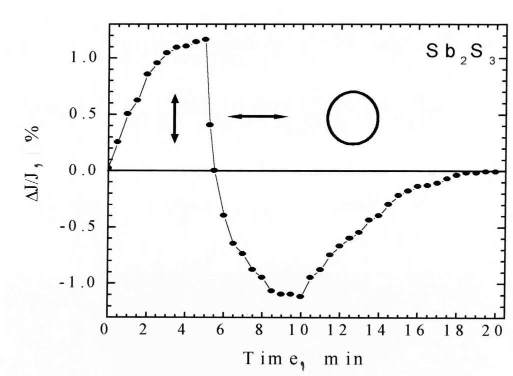

Fig. 9. Kinetics of relative anisotropy generated in 1.5 μm thick Sb_2S_3 film. Arrows and circle indicate the polarization state of the inducing He-Ne laser beam.

To the best of our knowledge, this is the first reported case of the photoinduced electrical anisotropy observation in the chalcogenide amorphous films. Since photoconductivity σ_{ph} is defined as a product of the concentration of photoexcited charge carriers n_{ph} and their mobility μ ($\sigma_{ph} = en_{ph}\mu$, where e is the electronic charge), either of these parameters can be responsible for the observed PA of photoconductivity. However in our experiments on photoconductivity, irradiation by the light of different polarizations but the same intensity generates the same n_{ph} and must not result in appearance of the photoelectrical anisotropy. Hence we conclude that the observed anisotropy of photoconductivity is due to different transport properties (mobility) of charge carriers at their movement in direction parallel or orthogonal to the electrical vector of inducing light. Therefore we observed the PA of carriers mobility μ ($\mu_x \neq \mu_y$). The obtained data indicate that the microanisotropic species, such as charged valence-alternation pairs, affect not only the light absorption process but also the process of transport of the non-equilibrium charge carriers (mobility of these carriers). While normally these microanisotropic species are oriented randomly that results in the isotropic photoconductivity, irradiation with linearly polarized light results in alignment of these species and respective anisotropic photoconductivity.

4. Polarization-dependent anisotropic photocrystallization

Our study of the polarized light interaction with ChGS films resulted in revealing new peculiarities in the phenomenon of photocrystallization of amorphous films. This phenomenon was discovered in 1968 [36] and then was studied already during more than 30 years. We found that the polarization state of the excited light influences the photocrystalization process and the properties of crystallized samples [37, 38]. Irradiation of glassy $Se_{70}Ag_{15}I_{15}$, Se and $Se_{20}Te_{20}$ films with linearly-polarized He-Ne- and Ar^{+}- laser light was shown to result in formation of polycrystalline films with strong optical anisotropy (dichroism), the sign of which is determined by the direction of the electrical vector of light. As it is seen from Fig. 10, the photoinduced dichroism excited by the He-Ne laser light in the $Se_{70}Ag_{15}I_{15}$ film at a constant direction of polarization vector, changed the sign very soon and grew slowly, achieving very large values of about 15 - 18 %. The sign of the final dichroism always was determined by the direction of the exciting light polarization vector. Final dichroism was stable and did not relax in the darkness. Annealing of irradiated films at glass transition temperature (55^{o} C) and at 80-90^{o} C for several hours did not lead to a destruction of photoinduced dichroism opposite to the situation in the AsSe films. Thus, all characteristics of PA in treated Se-Ag-I, $Se_{80}Te_{20}$ and a-Se films were different from those in films studied previously. The results obtained (unusual kinetics, another sign and large value of photoinduced dichroism, absence of relaxation and thermal destruction) permitted us to assume that we deal with photoinduced photocrystallization process. This assumption was confirmed by the direct structural investigations including optical microscopy, electron microscopy and X-ray diffraction study [37,38]. Thus, we observed the polarization-dependent laser-induced anisotropic photocrystallization of Se-Ag-I $Se_{80}Te_{20}$ and a-Se films. It is necessary to say that the same effect of polarization-dependent laser-induced photocrystallization of a-Se films was revealed approximately simultaneously and completely independently in two other groups [39, 40].

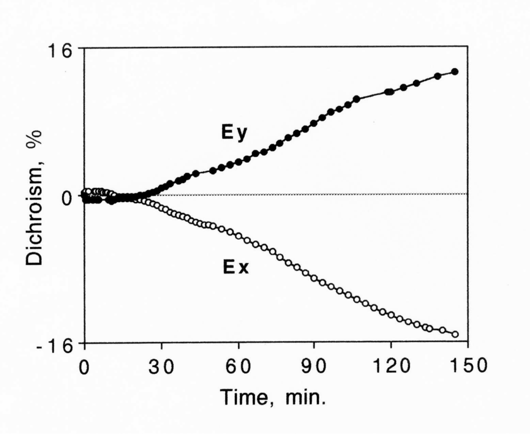

Fig. 10. Kinetics of dichroism generation in treated $Se_{70}Ag_{15}I_{15}$ film induced by a linearly polarized He-Ne laser beam with horizontal (Ex) and vertical (Ey) directions of the electrical vector.

5. Zn-photodoping

The photodoping of chalcogenide glassy semiconductors by silver has been the subject of numerous investigations. On the contrary, the photodoping of these materials by Zn is very poorly studied in spite of several important for practice peculiarities of the process in this case [41-43]. In our research we fulfilled more detailed investigation of Zn photodoping of some ChGS films [44,45]. Zn dissolution and Zn diffusion processes were investigated separately. For the Zn diffusion study we used two main methods: the recording of a rate of chalcogenide films etching in some liquid etchants and the Auger Electron Spectroscopy (AES) analysis combined with Ar sputtering depth profile, allowing to record the in-depth Zn distribution in the doped samples.

We confirmed that the photoinduced Zn dissolution in chalcogenide films proceeds only after heating to certain temperature. We determined these threshold temperatures of the Zn photodissolution beginning and also temperatures of the Zn thermodissolution beginning for all studied films. Then we studied the kinetics of Zn photodissolution at constant temperature for all structures investigated, using the parallel measurement of the changes in the light transmission of studied structure and the change of resistance of the Zn layer in this structure during the time of irradiation of the structure by the light of the Halogen lamp. The Zn photodissolution characteristics clearly show three stages of the process, namely, initial induction period, the stage of effective dissolution and the final stage, the tendency to saturation of dissolution just as well as it was observed at the Ag photodissolution in different chalcogenide glassy films. We clearly demonstrated the existence of the part of the constant photodissolution rate. This result permitted us to conclude that the rate-limiting step of the whole photodissolution process is the reaction at some interface: either Zn-chalcogenide film, or Zn-doped - non-doped interface.

The large difference was demonstrated for the Zn photodiffusion processes in structures fabricated by evaporation of Zn under and over the chalcogenide film.

The Auger spectroscopy study of the Zn depth profile for the Ni-As_2S_3-Zn-Ni samples, where Zn was evaporated over the As_2S_3 film, permits us to suppose that at photodiffusion, the amount of Zn is constant along whole diffusion area and that the sharp step-like profile of Zn exists just as it was shown for the Ag photodiffusion into chalcogenide films (Fig. 11a). In the case, where Zn was evaporated under the As_2S_3 film, we clearly showed the "tail" of the diffused Zn along the chalcogenide film (Fig. 11b). This difference of Zn diffusion processes in two different structures can be explained by various chemical reactions in two cases. We know that a vapour of As_2S_3 glass contains very different molecular complexes: S_8, AsS_3, AsS_5, As_2S_3, A_3S_4, As_2 etc. At the interaction of the vapour with Zn, different products such as ZnS, ZnAs and also different three-component products could appear which make difficult the next photoinduced movement of the Zn particles into the As_2S_3 film. For the case of the structure formed by Zn evaporation onto the As_2S_3 film, these intermediate compounds are not formed.

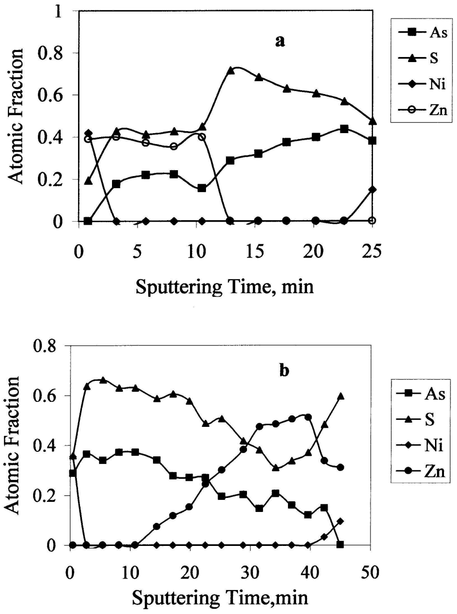

Fig. 11. Temporal variation of concentration of elements present in the Ni - As_2S_3 – Zn - Ni sample irradiated during 30 min for the cases where Zn was evaporated over the As_2S_3 film (a) and under the As_2S_3 film (b).

We started also the study of lateral Zn photodissolution in chalcogenide films and obtained the following interesting results: 1) In case of lateral Zn photodiffusion into As_2S_3 films (on the very thin Ni layers) we found a very high rate of the Zn diffusion >10 mm/hours. 2) photoinduced Zn diffusion is characterized not by diffusion front but by appearance of diffusion "tail". 3) The processes at the photodoped - non-doped interface determine the rate of the whole photodoping effect and just at this interface the light must be absorbed in order to provide effective Zn photodoping phenomenon.

Then we studied some chemical, electrical, photoelectrical and optical properties of the Zn-doped films. It was shown that these films could not be etched in all base-type etchants studied. The best results on the selective etching of Zn-doped and non-doped films were obtained with etchants on the base of isoamylamine or on the base of ethylenediamine. These results are the base for application of the Zn-photodoping process in the photolithography. The resistivity of the Zn-doped As_2S_3 films was shown to be ~10^{-6} $Ohm^{-1}cm^{-1}$. AC conductivity in the As_2S_3<Zn> film was characterized by appearance of the part of a nearly constant conductivity at $900\ Hz \le \omega \le 5\ kHz$, above which the conductivity increases proportionally to ω^n, where $n \le 1$. At $\omega < 400$ Hz we see the decrease of conductivity. This type of frequency dependence is typical of ionic conductivity.

In all Zn-photodoped films we observed and studied the photoconductivity. Both positive and negative photoconductivity was observed at different level of the excited light intensity.

The spectra of light transmission in the Zn-photodoped films were shown to have a shift to the long wave side to 50-100 nm in comparison with the spectra in the non-doped films. Using the well-known Swanepol method, we calculated the spectra of refractive index in the Zn-photodoped films. The photodoping was shown to result in increase of refractive index values to 0.2-04.

6. Application of ChGS for development of microlens arrays and photonic-band-gap structures

The inorganic photoresists based on the ChGS films were shown to have many interesting properties [46, 47]:

The variation of chalcogenide composition yields the photoresists sensitive to X-rays, UV, visible and near IR radiation and also to electron and ion beams.

Transition from positive to negative lithographic process with the same photoresist can be performed very easily by changing the composition of the developer.

All chalcogenide photoresists are characterized by extremely high resolution better than 0.1 μm.

The contrast characteristics: remaining photoresist thickness as a function of exposure energy, can be modified from steep to gentle slope by changing the maximum light intensity, exposure time and development time.

Optical transparency of all photoresists is high in the 0.8-12.0 μm range.

Refractive index of As-S, As-Se and As-Se-Te photoresists has high values between 2.3 and 3.2.

These properties not only can be used in usual photolithography of very high resolution but allow to find new application of chalcogenide photoresists. In usual photolithographic process, after obtaining with photoresist of necessary topology on the wafer, the organic photoresist is removed. The chalcogenide photoresist can be kept and work in the created IR optical device, as it is sufficiently stable and continues to have good optical properties. Below we will consider two examples of such applications of ChGS photoresists in microoptics: for develoment of the microlens arrays and some photonic-band-gap structures.

6.1. Microlens arrays

Microlens and microlens arrays can be found in an increasing number of optoelectronic applications, such as optical communication and computing, CCD cameras, faxes, imaging systems and IR technology. Microlens arrays have been fabricated by a variety of techniques, but the most common and widely used technique is photolithography in which the photosensitive material that is deposited on the substrate is exposed through a mask by tailored light distribution. Usually 3D-structures having the form of the microlens arrays are generated in a photoresist material and then transferred by anisotropic etching into a robust material transparent in the spectral range for which the microlens arrays are intended. Anisotropic etching is not a very simple process, therefore its elimination would be very desirable in the microlenses fabrication.

We proposed a new technology for fabrication of the IR microlens arrays which has the potential to eliminate this process step [47, 48]. This technology is based on the use of chalcogenide glasses that are simultaneously effective photoresists and very good IR optical materials. The method proposed is essentially the direct one-step formation of a 3D microlens array using dependence of the etching rate on the illumination intensity (above-mentioned specificity of the contrast characteristics) of chalcogenide photoresists. Cylindrical IR microlens arrays were successfully fabricated using the above discussed technique with As-S and As-Se photoresists [47, 48]. Following parameters were typical for microlens arrays made with As-S photoresist of 0.35 μm thickness: diameter of single lens is 12 μm, pitch is 12 μm, focal length (for λ = 500 nm) is 34 μm, array size is 40 × 40 microlenses, fill factor ia 97%.

In spite of many advantages, these microlens arrays also have some drawbacks. The maximum sag in such microlenses is limited to 1.3 μm and the focal length can be made much shorter if the sag is increased. The reason for the sag limitation is the photodarkening of the ChGS film upon exposure. The photodarkening effect does not present a problem when low sag values are desired (below 1.0-1.3 μm) but due to this effect there is a self-limitation process that limits the thickness that can be exposed. Another drawback in previously fabricated microlenses is a not very good shape of the convex surface formed in the direct one-step formation of microlenses. In order to overcome these drawbacks one can use the thermal reflow method that avoids exposure problems and leads to improvement of the shape of the lenses. Using a binary mask containing holes or slits, the islands of 3D binary shape can be formed that can be then transformed to 3D plano-convex microlenses. This is done by heating the material close to the melting point, causing reflow and formation of the desired 3D shape.

In our research [49] we used an ~820 nm $AsSeI_{0.1}$ photoresist which has comparatively low melting temperature. A contact binary photomask containing slits for cylindrical microlenses was used. Samples were exposed using a 200W halogen lamp and then developed in the negative photoresist mode in a monoethanolamine developer for 25 seconds in order to achieve 3D binary shapes. The thermal reflow procedure consisted of step heating of the binary shapes at intervals of 10 ^{o}C from 170 ^{o}C to 240 ^{o}C for 5 minutes at each interval. The microlenses obtained by the thermal reflow method had a very good convex surface.

The cylindrical microlens arrays had the following parameters: sag is 1.89 μm, length of single lens is 5 000 μm, width of single lens is 13.7 μm, pitch is 30 μm; focal length is 8 μm (for λ = 500 nm), array size: 50 × 5 (5 rows with 50 microlenses).

Later we succeeded to fabricate the IR microlens arrays of much bigger size using the thermal reflow technique due to development of new very effective selective developer on the base of isoamylamine. With this developer, having huge contrast value (100-250) even in the case of very thick As_2S_3 films, the sections of the film joined to the substrate are etched much slower than the non-irradiated As_2S_3 areas of the film.

Measurement of obtained circular and cylindrical microlens arrays were fulfilled with the help of the microinterferometer of "Zygo Corporation" (USA). The cylindrical microlens array is represented in Fig. 12. Quality of the convex surface of the microlenses (form, roughness) was very high and the reproducibility of the parameters of microlenses was also good.

The spherical microlens arrays had the following parameters: sag is 4.8 μm, diameter of single lens is 48.7 μm, pitch is 55 μm, focal length (for λ= 500 nm) is 47 μm, array size is 100 × 100 microlenses.

The cylindrical microlens arrays had the following parameters: sag is 5.34 μm, length of single lens is 2500 μm, width of single lens is 50.4 μm, pitch is 60 μm (horizontal axes) and 2550 mm (vertical axes), focal length is 46 μm (for λ= 500 nm), array size: 50 × 2 (2 rows with 50 microlenses).

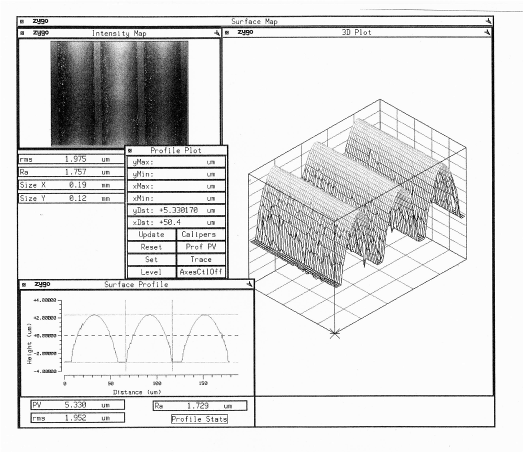

rms 1.975 um
Ra 1.757 um
Size X 0.19 mm
Size Y 0.12 mm
yDst: +5.330170 um
xDst: +50.4 um
PV 5.330 um
rms 1.952 um
Ra 1.729 um

Fig. 12. Array of cylindrical microlenses produced by the thermal reflow method.

6.2. Photonic-band-gap structures

Photonic crystals have been the object of intense activity. Their optical properties give them an advantage over the standard optical materials. For three-dimensional photonic crystals there are two main fabrication methods: self-assembly [50] and layer-by-layer construction [51]. The ChGS are highly promising material for fabrication of optical communication components due to the possibility to combine the advantages of layer-by-layer construction flexibility and cheap method of fabrication. We fabricated the three-dimensional photonic-band-gap structures on the base of the As-Se-Te films [52, 53]. We made a layer-by-layer construction, using the fact that the required structure is a superposition of diffraction grating stacked on the top of the other. Each layer is formed by vacuum evaporation of 0.3 μm $AsSeTe_{0.1}$ film, used as a negative photoresist, writing a holographic pattern by two-beam interference and etching of the non-illuminated parts. The grating obtained by this procedure is planarized using spin-coated organic Shipley`s photoresist, and the next layer is formed on the previous one. The direction of grating in the second layer is perpendicular to the first one. In subsequent odd layers, the direction is parallel to the first one, and in the even layers - to the second. In addition, the half period phase shift exists between each two nearest parallel layers. This alignment was done using the interference properties of the structure. Finally, the photoresist can be washed out by acetone, remaining the $AsSeTe_{0.1}$ structure. The example of the four-layer structure is shown in Fig. 13.

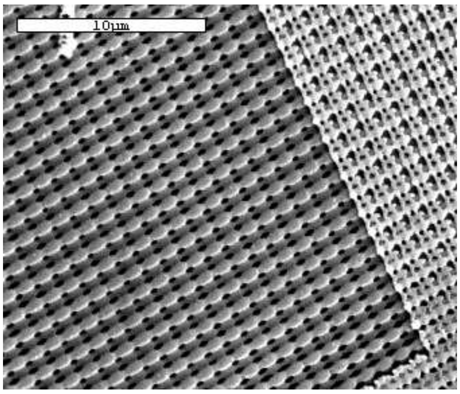

Fig. 13. Four-layer photonic-band-gap structure based on $AsSeTe_{0.1}$ films.

Another way to apply the ChGS for creating of the photonic crystals is the fabrication of composite opal structures with a high potential for nonlinear optical application by infiltration with chalcogenide glasses by precipitation from solution. The first such structures were performed in our experiments, in which we used the solutions of As_2S_3 and $As_{50}Se_{50}$ glasses in ethylenediamine [54].

Additionally we want to mention our recent results in application of ChGS for linear holographic recording [55,56] and for sub-wavelength optical recording [57].

7. Conclusion

Results of the research fulfilled in the Ben-Gurion University during last ten years demonstrate that the ChGS continue to be very promising non-crystalline materials. They display different new interesting physical phenomena, which are not observed in other semiconducting materials. These chalcogenide materials open new possibilities in development of different efficient electro-optical devices. Particularly, we can hope that in near future the ChGS will allow to develop new devices for optical communication systems.

The authors are very glad to participate with this review paper in the Festschrift dedicated to the 80th Jubilee of Stan Ovshinsky. His pioneering scientific and engineering activity substantially helped to development of new field of physics and technology of non-crystalline semiconducting and optical materials, to creating of new devices, applied in different fields of modern engineering.

One of us (V.L.) has long experience of pleasant and productive meetings with Stan, starting from the first Meeting on Glassy Semiconductors, organized by Professor Boris Kolomiets in Leningrad in 1967. We wish to Stan Ovshinsky to be healthy and to make many new interesting researches and discoveries.

Acknowledgements

We want to thank all colleagues both in the Ben-Gurion University and in other research centers who participated in our study of ChGS. We also thank the Israel Science Foundation and Israeli Ministry of Science for their support of this research.

References

[1] A. E. Owen, A. P. Firth, P. J. S. Even, Philos. Mag. **B 52**, 347, (1985).
[2] S. R. Elliott, J. Non-Cryst. Sol. **81**, 71 (1986).
[3] V. M. Lyubin, J. Non-Cryst. Sol. **97&98**, 47 (1987).
[4] H. Fritzsche, Philos. Mag. **B 68**, 561 (1993).
[5] K. Tanaka, Rev. Sol. St. Sci. **4**, 641 (1990).
[6] K. Shimakawa, A. Kolobov, S. R. Elliott, Adv. in Phys. **44**, 475 (1995).
[7] Yu. A. Bykovskii, A. I. Maimistov, A. V. Mironos, V. L. Smirno, Sov. J. Quantum Electron. **12**, 488 (1982).
[8] A. V. Kolobov, N. Sebastian, Sov. Phys. Tech. Phys. **29**, 106 (1984).
[9] G. Vartman, R. V. Danelus, Yu. Kluge, A. O. Ozols, Avtometrija No. 1, 80 (1987).
[10] E. G. Barash, A. Yu. Kabin, V. M. Lyubin, R. P. Seisyan, Sov. Phys. Tech. Phys. **37**, 292 (1992).
[11] Y. Aoyagi, Y. Segawa, S. Namba, T. Suhara, H. Nishihara, H. Gamo, Phys. Stat. Sol.(a) **67**, 669 (1981).
[12] K. Tanaka, J. Appl. Phys. **65**, 2042 (1989).
[13] I. Bar, M. Klebanov, V. Lyubin, S. Rosenwaks, S. Shtutina, V. Volterra, Proc. SPIE 1972, 251 (1992).
[14] M. Klebanov, S. Shtutina, I. Bar, V. Lyubin, S. Rosenwaks, V. Volterra, Proc. SPIE 2426, 198 (1995).
[15] G. Rosenblum, B. G. Sfez, Z. Kotler, V. Lyubin, M. Klebanov, Appl. Phys. Lett. **75**, 3249 (1999).
[16] B. G. Sfez, G. Rosenblum, Z. Kotler, V. Lyubin, M. Klebanov, Materials Science in Semiconductor Processing **3**, 499 (2000).

[17] V. G. Zhdanov, V. K. Malinovskii, Sov. Tech. Phys. Lett. **3**, 943 (1977).

[18] V. G. Zhdanov, B. T. Kolomiets, V. M. Lyubin, V. K. Malinovskii, Phys. Stat. Sol. (a) **52**, 621 (1979).

[19] R. Grigorovici, A. Vancu, L. Ghita, J. Non-Cryst. Sol. **59-60**, 903 (1983).

[20] K. Kimura, K. Murayama, T. Ninomiya, J. Non-Cryst. Sol. **77-78**, 1203 (1985).

[21] J. M. Lee, M. A. Paesler, J. Non-Cryst. Sol. **97-98**, 1235 (1987).

[22] V. M. Lyubin, V. K. Tikhomirov, J. Non-Cryst. Sol. **114**, 133 (1989).

[23] V. K. Tikhomirov, S. R. Elliott, Phys. Rev. **B 51**, 5538 (1995).

[24] V. M. Lyubin, V. K. Tikhomirov, J. Non- Cryst. Sol. **135**, 37 (1991).

[25] V. K.Tikhomirov, S. R. Elliott, Phys. Rev. **B 49**, 1746 (1994).

[26] K. Tanaka, M. Notani, H. Hisakuni, Sol. St. Commun. **95**, 461 (1995).

[27] T. Kosa, I. Janossy, Phil. Mag. **B 64**, 355 (1991).

[28] H. Fritzsche, J. Non-Cryst. Sol. **164-166**, 1169 (1993).

[29] V. M. Lyubin, M. L. Klebanov, Semiconductors **32**, 817 (1998).

[30] V. Lyubin, M. Klebanov, Phys. Rev. **B 53**, 11924 (1996).

[31] V. L. Averyanov, A. V. Kolobov, B. T. Kolomiets, V. M. Lyubin, Phys. Stat. Sol. **A 57**, 81 (1980).

[32] V. Lyubin, M. Klebanov, S. Rosenwaks, V. Volterra, J. Non-Cryst. Sol. **164-166**, 1165 (1993).

[33] A. V. Kolobov, V. Lyubin, T. Yasuda, M. Klebanov, K. Tanaka, Phys. Rev. **B 55**, 8788 (1997).

[34] V. Lyubin, M. Klebanov, V. K. Tikhomirov, Phys. Rev. Lett. **87**, 216806 (2001).

[35] V. Lyubin, M. Klebanov, J. Optoel. Adv. Mat. **3**, 265 (2001).

[36] J. Dresner, G. B. Stringfellow, J. Phys. Chem. Sol. **29**, 303 (1968).

[37] V. Lyubin, M. Klebanov, M. Mitkova Petkova, Appl. Phys. Lett. **71**, 2118 (1997).

[38] V. Lyubin, M. Klebanov, M. Mitkova Petkova, J. Non-Cryst. Sol. **227-230**, 739 (1998).

[39] K. Ishida, K. Tanaka, Phys. Rev. **B 56**, 206 (1997).

[40] V. K. Tikhomirov, P. Hertogen, C. Glorieux, G. I. Adriaenssens, Phys. Stat. Sol. **A 162**, R1 (1997).

[41] A. V. Kolobov, B. T. Kolomiets, V. M. Lyubin, M. A. Tagirdzhanov, Solid State Comm. **54**, 379 (1985).

[42] V. M. Lyubin, A. V. Kolobov, J. Non-Cryst. Sol. **90**, 489 (1987).

[43] A. V. Kolobov, G. E. Bedelbaeva, Phil. Mag. **B 64**, 91 (1991).

[44] A. Arsh, N. Froumin, M. Klebanov, V. Lyubin, J. Optoel. Adv. Mat. **4**, 27 (2002).

[45] V. Lyubin, M. Klebanov, A. Arsh, N. Froumin, A. V. Kolobov, J. Non-Cryst. Sol. (to be published).

[46] V. M. Lyubn, A. M. Sedikh, N. N. Smirnova, V. P. Shilo, Microelectronics (USSR) **18**, 523 (1989).

[47] N. P. Eisenberg, M. Manevich, M. Klebanov, V. Lyubin, S. Shtutina, J. Non-Cryst. Sol. **198-200**, 766 (1996).

[48] V. Lyubin, M. Klebanov, I. Bar, S. Rosenwaks, N. P. Eisenberg, M. Manevich, J. Vac. Sci. Technol. **B 15**, 823 (1997).

[49] S. Noach, M. Manevich, M. Klebanov, V. Lyubin, N. P. Eisenberg, Proc SPIE 3778, 151 (1999).

[50] Y. A. Vlasov, V. N. Astratov, O. Z. Kaminov, A. A. Kaplyanskii, V. N. Bogomolov, A. V. Prokofiev, Phys. Rev. **B 55**, 1335 (1997).

[51] K. M. Ho, T. Chan, C. M. Soukoulis, R. Biswas, M. Sigalis, Solid State Commun. **89**, 413 (1994).

[52] A. Fegel, Z. Kotler, B. Sfez, A. Arsh, M. Klebanov, V. Lyubin, Appl. Phys. Lett. **77**, 3221 (2000).

[53] A. Fegel, Z. Kotler, B. Sfez, A. Arsh, M. Klebanov, V. Lyubin, Proc. SPIE 4277, 249 (2001).

[54] V. N. Astratov, A. Madaqwi, M. S. Skolnick, V. K. Tikhomirov, V. Lyubin, D. G. Lidzey, M. Ariu, A. L. Reynolds, Appl. Phys. Lett. **78**, 4094 (2001).

[55] B. Spektor, M. Lisiansky, J. Shamir, M. Klebanov, V. Lyubin, Appl. Phys. Lett. **76**, 798 (2000).

[56] B. Spektor, M. Lisiansky, J. Shamir, M. Klebanov, V. Lyubin, J. Appl. Phys. **87**, 3234 (2000).

[57] Y. Isbi, Sh. Sternklar, E. Granot, V. Lyubin, M. Klebanov, A. Lewis, Optics Commun. **171**, 219 (1999).